Applied Catalysis B: Environmental 115–116 (2012) 190–200

Contents lists available at SciVerse ScienceDirect

Applied Catalysis B: Environmental

journal homepage: www.elsevier.com/locate/apcatb

Effect of a second metal (Y, K, Ca, Mn or Cu) addition on the carbon dioxide reforming of methane over nanostructured palladium catalysts

Chunkai Shi [a,*], Peng Zhang [b,**]

[a] Petroleum Recovery Research Center, New Mexico Tech, Socorro, NM 87801, USA
[b] Department of Chemistry, University of Cincinnati, Cincinnati, OH 45221, USA

ARTICLE INFO

Article history:
Received 24 August 2011
Received in revised form
23 November 2011
Accepted 1 December 2011
Available online 9 December 2011

Keywords:
CO_2 reforming of CH_4
Palladium catalysts
Yttrium
Potassium
Calcium
Manganese
Copper
Carbon deposition

ABSTRACT

The CO_2 reforming of CH_4 to synthesis gas was investigated over nanostructured Pd/Al_2O_3 catalysts promoted by various additives (K, Ca, Y, Mn and Cu) using a stoichiometric feedstock mixture. In order to understand the effect of the additives on the surface properties and catalytic performance of the catalysts, fresh and spent samples were characterized by a number of techniques, such as N_2 adsorption-desorption isotherms, XRD, CO-chemisorption, H_2-TPR, TPO, Raman and TEM. Additives strongly modified the reduction properties of Pd species and metal surface dispersion. The results showed that the addition of Y or Ca to Pd/Al_2O_3 slightly increased the initial activity expressed as CH_4 and CO_2 conversions, which is attributed to decreased reducibility of Pd species and enhanced Pd dispersion. In contrast, while the addition of K, Mn and Cu similarly reduced the reducibility of Pd species, their surface metal dispersions apparently decreased owing to decoration effect or alloy formation. This leads to lower initial activities for the modified catalysts than Pd/Al_2O_3. On the other hand, stability of catalysts activity during the long-term tests was associated with Pd sintering resistance as well as carbon deposition. The CO_2 reforming of CH_4 was ceased over Pd/Al_2O_3 after around 4.5 h of reaction due to catalyst bed blockage caused by the large amount of carbon deposition. The carbon formation was accelerated by Pd sintering. Among all catalysts, Y-modified Pd/Al_2O_3 showed the best stability with almost no activity loss in 20 h of reaction. This is probably because that the addition of Y to Pd/Al_2O_3 notably suppresses carbon formation and metal sintering and maintains Pd particle size below 10 nm. This particle size is crucial, below which carbon formation can be completely avoided under the present reforming conditions. For catalysts with other additives the catalytic activities decreased to different degrees after long-term tests, due to metal sintering and carbon deposition.

1. Introduction

Recently reforming of methane with carbon dioxide (also known as dry reforming of methane: $CH_4 + CO_2 \rightarrow 2H_2 + 2CO$, $\Delta H_{298}^{\circ} = +247\ kJ\ mol^{-1}$) has attracted increasing attention as it consumes two of the most important greenhouse gases to produce synthesis gas (syngas), a mixture of CO and H_2, which is industrially useful for making various value-added liquid hydrocarbons and oxygenates through the well-known Fischer–Tropsch (FT) synthesis process [1,2]. The reforming process is also regarded as the most cost-effective way to obtain H_2 source [3]. Most group VIII metals are more or less active for the reaction [1,2]. However, no successful industrial application in large scale has been reported so far due to the lack of development of appropriate catalysts. A major drawback of the dry reforming of CH_4 is the requirement of high operation temperature, usually above 800 °C, to achieve high enough conversions of both CH_4 and CO_2 due to the strong endothermic nature of the reaction. Supported Ni and Co catalysts have been extensively investigated for this reaction due to their low cost and availability in large scale. Yet mono-component Ni or Co catalysts require high reaction temperature for high conversion. The harsh reaction conditions usually lead to the sintering of active metal component and the occurrence of a large amount of carbon deposition on the catalyst surface, resulting in catalyst deactivation, reactor blocking and catalyst breakdown [1,2,4,5].

In order to overcome the drawbacks, a promising approach is the addition of various promoters to Ni or Co catalysts to improve their catalytic performance. K, Ca, Mn, Fe, Cu, Y, La and Ce were frequently added to supported Ni or Co catalysts for improving metal dispersion, decreasing carbon deposition and/or enhancing activity stability [6–10]. Nevertheless, catalyst deactivation remains as a serious problem, and a high reaction temperature

* Corresponding author.
** Corresponding author. Fax: +1 513 556 9239.
E-mail addresses: chunkaishi@yahoo.com, cshi@nmt.edu (C. Shi), peng.zhang@uc.edu (P. Zhang).

0926-3373/$ – see front matter © 2011 Elsevier B.V. All rights reserved.
doi:10.1016/j.apcatb.2011.12.002

(above 750 °C) is still needed to achieve high conversions of CO_2 and CH_4. Therefore, development of catalysts with good catalytic performance at lower reaction temperature is of great interest for the process.

Depending on supports and promoters, Rh, Pt and Pd catalysts have demonstrated excellent activity, selectivity and stability with strong resistance to carbon deposition for the drying reforming of CH_4 [1,2,11,12]. In particular, Pd-based catalysts with low metal loading are very attractive, because Pd is much less inexpensive than other noble metals such as Pt and Rh. It also has a very strong capability to activate CH_4 as well as excellent activity for CH_4 reforming by CO_2 at lower temperatures [13–16]. Yamaguchi and Iglesia [16] have reported that supported Pd catalyst is most active for the C—H bond activation of CH_4 compared to other Group VIII metal catalysts. The C—H bond activation is suggested as the rate limiting step for CH_4 reforming reaction [1]. SiO_2-supported Pd catalyst was observed to decompose CH_4 to H_2 and carbon deposit at around 250 °C [14]. The catalytic activity of Al_2O_3 and TiO_2-supported Pt group metal catalysts were investigated for CO_2 reforming of CH_4, and Pd and Rh showed close activities at 500 °C [13]. In addition, there are reports in the literature that Al_2O_3-supported Pd catalysts are very active and selective in the range of 400–730 °C for the reforming reaction [15,17]. However, unpromoted Pd catalysts suffered rapid deactivation at elevated reaction temperature (>600 °C) due to serious metal sintering and significant carbon formation during long-term stability test [17]. Supports and promoters have been, therefore, adopted to effectively suppress carbon formation [16–18], as they can effectively activate CO_2 and remove carbon species at the metal/support interface via reaction between produced active oxygen and chemisorbed carbon. On the other hand, exposed small Pd particle size, i.e. high Pd dispersion, could play a key role in obtaining high activity, selectivity and stability for the reforming reaction since CH_4 decomposition is a sensitive reaction on metal surface. It was demonstrated that additives of La and Ce effectively retarded Pd and Pt metal sintering and enhanced the active metal surface for the dry reforming of CH_4 [11,17,19]. And small metal particle size also tends to increase CO_2 activation on support [20]. In addition, nanostructured γ-Al_2O_3-supported Pt catalyst has been shown to be highly stable and active catalyst in CO_2 reforming of CH_4 [21].

We thus envision that low Pd loading catalyst, combined with excellent promoter and industrially available inexpensive support, could be an optimal candidate as effective and efficient catalyst of dry reforming of CH_4. In this study, effect of various additives, i.e. K, Ca, Y, Mn and Cu, on activity, selectivity and stability of nanostructured γ-Al_2O_3-supported 1 wt.% Pd catalyst for dry reforming of CH_4 is investigated at atmospheric pressure. To our best knowledge, these modified Pd catalysts for dry reforming of CH_4 have not been reported in the literature. Additives are expected to modify the surface properties of Pd active component, resulting in different performance of catalysts. Fresh and spent catalysts were characterized thoroughly by BET surface area, chemisorption, H_2-TPR, XRD, TPO, Raman and TEM to obtain insight of both initial activity and stability of catalysts.

2. Experimental

2.1. Catalyst preparation

Commercially available nanostructurd γ-alumina (Alfa Aesar, 1/8 in. pellet) was crushed and sieved to obtain particles of 20–40 mesh sizes. Additive-added Pd catalyst precursors were prepared by equal volume co-impregnation technique in one step using an aqueous solution of Pd and additive nitrates, i.e. $Pd(NO_3)_2{\cdot}xH_2O$ (containing 38 wt.% metallic Pd), KNO_3, $Ca(NO_3)_2{\cdot}4H_2O$, $Y(NO_3)_3{\cdot}6H_2O$, $Mn(NO_3)_2{\cdot}6H_2O$ and $Cu(NO_3)_2{\cdot}3H_2O$ (all from Alfa Aesar), to obtain metallic Pd and additive loadings of 1 and 5 wt.%, respectively. After impregnation, the catalyst was kept at room temperature for 12 h, followed by drying at 120 °C for another 12 h and calcining at 500 °C for 3 h in static air. Catalysts are designated as Pd5 M/Al_2O_3 where M = Y, K, Ca, Mn or Cu.

2.2. Catalyst characterization

The surface textural properties of samples were tested at liquid nitrogen temperature using a Micromeritics ASAP-2020 instrument. The samples were degassed at 300 °C for 4 h prior to testing to remove any adsorbed moisture. The specific surface area was determined using the standard Brunauer–Emmett–Teller (BET) method in the pressure interval of 0.03–0.3 P/P°, and the pore distribution was calculated using the Barrett–Joyner–Halenda (BJH) method from the adsorption branch of the N_2 isotherm.

X-ray powder diffraction patterns of samples were recorded on a Philips X'Pert diffractometer using Cu Kα radiation (λ = 1.5418 Å) in θ–2θ scan mode, operated at 45 kV and 40 mA. Step size and step scan time are 0.02° and 3 s, respectively. The average crystallite size of metallic Pd was calculated using the Scherrer equation.

The CO chemisorption of samples reduced before reaction was measured using the Micromeritics ASAP-2020 instrument to determine the Pd dispersion and surface metal area. The sample was first degassed at 400 °C for 4 h and then cooled down, weighted and moved to a U-shape measurement tube. Prior to CO chemisorption, the sample was evacuated at 100 °C for 1 h, followed by in situ reducing in hydrogen at 400 °C for 2 h and then evacuating at 100 °C for another hour. Finally, the isotherm of CO chemisorption was measured at 35 °C. The Pd dispersion and surface metal area were calculated assuming the stoichiometry of Pd/H = 1.

The reducibility of sample was performed by a hydrogen temperature-programmed reduction (H_2-TPR) method. Approximately 100 mg of sample was loaded into a quartz tube reactor with a K-type thermocouple contacting the bottom of sample layer. Prior to hydrogen reduction, the sample was purged with UHP nitrogen flow of 30 ml/min for 1 h at room temperature. The H_2-TPR run was carried out by heating the sample in 5% H_2/N_2 atmosphere at a ramp rate of 10 °C/min. The hydrogen consumption was monitored by a QSM200 mass spectrometer (SRS, Inc.).

Carbon species deposited on the catalyst during dry reforming reaction was studied by temperature-programmed oxidation (TPO) method. Approximately 50 mg of sample was loaded into the aforementioned quartz micro-reactor. After purged in a dry air flow (25 ml/min) for 30 min, the sample was heated in same air flow from room temperature to 850 °C at a ramp rate of 10 °C/min. The reaction product, CO_2 (m/e = 44), was monitored using the aforementioned mass spectrometer. The amount of carbon deposition was estimated from the obtained CO_2 peak area, which was quantified by using the peak area of known volumes of CO_2.

Raman spectra of spent catalyst was obtained using a LabRAM Raman microscope (HORIBA Jobin Yvon Inc.) with the following operation parameters: a He–Ne laser of 632.8 nm as excitation source, laser intensity of ~2 mW, 10 s acquisition time and a total of 30 accumulation per spectrum. Before sample measurement, Raman spectrum was calibrated using a silicon wafer peak at 520.7 cm^{-1}. All the samples were analyzed under an atmospheric condition without pre-treatment.

TEM images of spent catalysts were obtained on a JEOL 2010 instrument operated at an accelerating voltage of 200 kV. The sample was prepared by dropping and drying the spent catalyst, which was dispersed in anhydrous ethanol by sonication, on holey carbon-coated Cu grids.

2.3. Catalytic reaction

The carbon dioxide reforming of methane was carried out in a fixed-bed quartz micro-reactor at atmospheric pressure. All gas flow rates were controlled by GFC mass flow controllers (Aalborg Inc.). Typically, 100 mg of sample was loaded into the reactor of 4 mm ID. Sample temperature was controlled using a K-type thermocouple contacting the bottom of sample layer. Before reaction, sample was in situ reduced in UHP H_2 with a flow rate of 13 ml/min at 500 °C for 2 h and then cooled down to room temperature in the same gas flow. After purged by He (20 ml/min) for 30 min, the mixed feedstock gases (CH_4 = 10 ml/min, CO_2 = 10 ml/min and He = 20 ml/min) were introduced to the catalyst bed, and the reaction was conducted at a ramp rate of 10 °C/min. For stability test, the reaction temperature was hold at 700 °C for desired time. Feedstock and product gases were simultaneously measured by a QMS200 mass spectrometer (SRS Inc.) with capillary sampling and a gas chromatograph (Buck 910) equipped with a CARBOXEN 1000 column and a TCD. The detected mass-to-charger ratios (M/Q) are 44, 2, 28 and 15 for CO_2, H_2, CO and CH_4, respectively. A data collection mode of pressure via time (P vs T) is used for a continuous on-line monitoring of various gas constituents. The conversions (X_{CH_4} and X_{CO_2}) of CH_4 and CO_2 as well as the ratio of H_2 and CO selectivity (H_2/CO) were calculated using the following Eqs. (1)–(3). As an example $[CH_4]_{in}$ and $[CH_4]_{out}$ stand for the concentrations of CH_4 in feedstock and product gases, respectively. The concentrations of all components are in mol%.

$$X_{CH_4} = \frac{[CH_4]_{in} - [CH_4]_{out}}{[CH_4]_{in}} \times 100\% \quad (1)$$

$$X_{CO_2} = \frac{[CO_2]_{in} - [CO_2]_{out}}{[CO_2]_{in}} \times 100\% \quad (2)$$

$$H_2/CO = \frac{[H_2]_{out}}{2[CO]_{out} \times ([CH_4]_{in} - [CH_4]_{out})} \times ([CH_4]_{in} - [CH_4]_{out} + [CO_2]_{in} - [CO_2]_{out}) \quad (3)$$

3. Results and discussion

3.1. Characterization of catalyst before reaction

3.1.1. Textural properties

Table 1 shows the results of nitrogen physisorption obtained for all catalysts and Al_2O_3 support. Al_2O_3 and Pd/Al_2O_3 show similar values of BET surface area, pore volume and pore size, indicating that 1% Pd loading has no apparent effect on the textural characteristics of the support. After co-impregnation with 1 wt.% Pd and 5 wt.% metal additive loadings, the BET surface areas of $Pd5Y/Al_2O_3$, $Pd5Mn/Al_2O_3$ and $Pd5Cu/Al_2O_3$ decreased by 11–13 m^2/g compared to Pd/Al_2O_3, whereas those of $Pd5K/Al_2O_3$ and $Pd5Ca/Al_2O_3$ catalysts dropped by 20 m^2/g. The slightly larger decrease for the last two catalysts could be due to both stronger basicity and larger molar amounts of K and Ca than that of other promoters. Moreover, additive-added samples show slight decrease in pore volume and pore size than Pd/Al_2O_3, yet no obvious difference is observed among all promoted Pd catalysts.

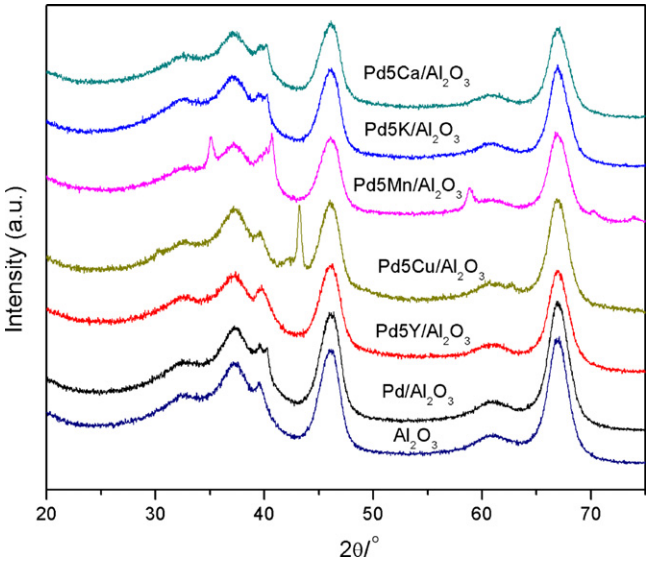

Fig. 1. The XRD profiles of catalysts reduced before reaction.

3.1.2. XRD

The structure and components of Pd catalysts reduced before reaction were characterized by XRD (Fig. 1). All catalysts show a clear γ-Al_2O_3 structure as reflected in the X-ray diffraction peaks at 2θ = 66.7°, 45.8° and 37.6° (JCPDS 10-0425). Except for $Pd5Cu/Al_2O_3$, profiles of all samples contain a diffraction peak (2θ = 40.1°) associated with metal Pd (1 1 1) phase (JCPDS 05-0681). Based on the Scherrer equation, the average Pd crystallite size of catalyst is calculated using the full width at half maximum (FWHM) of the peak, corrected by subtracting the corresponding diffraction peak of γ-Al_2O_3. The resulting values of Pd crystallite size are 16.5, 5.1, 14.3, 8.9 and 15.0 nm for Pd/Al_2O_3, $Pd5Y/Al_2O_3$, $Pd5K/Al_2O_3$, $Pd5Ca/Al_2O_3$ and $Pd5Mn/Al_2O_3$, respectively (Table 2). Apparently, the selected additives can significantly influence the Pd crystallite size of catalysts. $Pd5Y/Al_2O_3$ shows the smallest size as compared with Pd/Al_2O_3, suggesting that Y greatly strengthen the interaction between Pd and the support. As for $Pd5Cu/Al_2O_3$, no Pd diffraction peak is observed, but a bimetallic Pd–Cu alloy component can be identified by diffraction peaks at 2θ = 42.6° and 61.8° (JCPDS 057-0606). The observation agrees well with the reported literature [22]. The average crystallite size for the Pd–Cu alloy calculated by Scherrer equation is 6.5 nm. Meanwhile, $Pd5Cu/Al_2O_3$ also exhibits an intense peak at 2θ = 43.27°, assigned to metal Cu (JCPDS 002-1225). This means that only part of Cu binds to Pd to form Pd–Cu alloy due to much more loaded Cu than Pd. In addition to the peaks ascribed to Pd and γ-Al_2O_3, other diffraction peaks (2θ = 35.07°,

Table 1
Textural properties of support and catalysts.

Sample	BET surface area (m^2/g)		Pore volume (cm^3/g)		Pore size (nm)	
	Before reaction	After reaction	Before reaction	After reaction	Before reaction	After reaction
γ-Al_2O_3	206.7	–	0.603	–	12.21	–
Pd/Al_2O_3	205.8	157.5	0.595	0.398	12.07	10.81
$Pd5Y/Al_2O_3$	193.1	180.4	0.545	0.525	11.82	11.63
$Pd5K/Al_2O_3$	185.4	168.6	0.545	0.419	12.18	10.84
$Pd5Ca/Al_2O_3$	186.5	171.8	0.534	0.445	11.87	11.54
$Pd5Mn/Al_2O_3$	194.3	175.5	0.547	0.483	11.80	11.68
$Pd5Cu/Al_2O_3$	192.0	172.1	0.548	0.478	11.97	11.68

Table 2
The Pd dispersion, metal area and particle size of catalysts.

Sample	Pd dispersion (%)	Metal surface area (m^2/g sample)	Pd particle size (nm)	
			$D1_{XRD}$[a]	$D2_{XRD}$[a]
Pd/Al_2O_3	23.4	1.057	16.5	28.6
$Pd5Y/Al_2O_3$	33.1	1.489	5.1	10.6
$Pd5K/Al_2O_3$	18.1	0.837	14.3	26.4
$Pd5Ca/Al_2O_3$	29.2	1.328	8.9	16.7
$Pd5Mn/Al_2O_3$	18.6	0.842	15.0	20.7
$Pd5Cu/Al_2O_3$	12.3	0.457	–	–

[a] D1 and D2 stand for the Pd particle sizes of catalysts determined by XRD before and after reaction, respectively.

40.75°, 58.87°, 70.2° and 74.0°) also appear in the $Pd5Mn/Al_2O_3$ pattern, which can be related to the cubic MnO phase (JCPDS 01-075-0625). This confirms that Mn oxide precursor was reduced to MnO after H_2 treatment, well in consistent with the reported literatures [23].

3.1.3. CO-chemisorption

Surface property of the active component is more important than its bulk property, because accessible active component is closely related to the catalytic performance of supported catalyst. Table 2 lists the Pd dispersion and metal area values of the reduced catalysts determined by the amounts of irreversibly adsorbed CO. There is a notable change in terms of Pd dispersion and metal area as a result of the different additives to Pd/Al_2O_3. $Pd5Y/Al_2O_3$ shows the highest Pd dispersion value (33.1%) as compared to Pd/Al_2O_3, which has a Pd dispersion value of 23.4%. Conversely, $Pd5Cu/Al_2O_3$ displays the lowest Pd dispersion value of 12.3% among all samples. The Pd dispersion and metal area of catalysts decrease in the order of: $Pd5Y/Al_2O_3 > Pd5Ca/Al_2O_3 > Pd/Al_2O_3 > Pd5Mn/Al_2O_3 \sim Pd5K/Al_2O_3 > Pd5Cu/Al_2O_3$. Generally, agglomeration of surface active metal component due to sintering would result in an increased particle size and a decreased surface dispersion and metal area, indicating an inverse relationship between the surface dispersion/metal area of active component and its particle size. However, one can see from Table 2 that the inverse relationship does not always maintain in the present catalyst system. For example, Pd/Al_2O_3, $Pd5K/Al_2O_3$ and $Pd5Mn/Al_2O_3$ have similar Pd crystallite sizes, but K, or Mn-added catalysts show smaller Pd dispersion values than Pd/Al_2O_3. Consider the catalyst preparation includes co-impregnation of both Pd and excessive additive to the support, the finding could be ascribed to the decoration effect caused by K or Mn species covering part of Pd species, resulting in the decrease of exposed metal area and number of surface Pd atom. Moreover, Pd–Cu alloy formation on $Pd5Cu/Al_2O_3$ leads to more reduction in terms of exposed metal area and number of surface Pd atom, showing a stronger covering effect produced by the chemical combination of Cu and Pd than the aforementioned decoration effect. On the other hand, for $Pd5Y/Al_2O_3$ and $Pd5Ca/Al_2O_3$, it may be difficult to determine whether there exists a decoration effect between Pd and additives from the XRD and chemisorption results. Pd/Al_2O_3 catalysts with or without Y or Ca additives qualitatively comply with the inverse relationship between Pd dispersion/metal area and metal crystallite size, i.e. Y and Ca-promoted catalysts display smaller crystallite sizes and higher Pd dispersion/metal area values than the unpromoted ones.

3.1.4. H_2-TPR

Fig. 2 compares the reducibility of calcined samples. Pd/Al_2O_3 only shows a negative hydrogen consumption peak at 66 °C, which is associated with the decomposition of β-palladium hydride. The hydride is formed by low temperature-reduced metal Pd adsorbing hydrogen and decomposes to release hydrogen in enhanced temperature [24,25]. This observation implies that palladium oxide on Pd/Al_2O_3 can be completely reduced at room temperature when purged in hydrogen flow prior to H_2-TPR start, suggesting that a weak interaction occur between Pd and support and lead to Pd species to be reduced easily. This is consistent with the relatively large particle size of unpromoted Pd on Pd/Al_2O_3 (Table 2).

Note that H_2-TPR profiles of all additive-added Pd catalysts display positive hydrogen consumption peaks, indicating that additives greatly lower the reducibility of Pd precursor. It is well known that strong interaction between palladium oxide and additive-added support could significantly increase the reduction temperature of Pd precursors [26,27], depending on the nature of the additives. Meanwhile, decoration effect and alloy formation would also increase the reduction temperature of Pd-containing precursors during the reduction process. On the other hand, the addition of noble metals (such as Pd and Ru) to transition metal, alkali or alkaline earth metal-modified supports significantly improves the reduction of the additive species, and the reduction is assisted by a hydrogen spillover from noble metal to additives [23,26–29].

The profile of $Pd5Y/Al_2O_3$ contains a narrow reduction peak at 72.6 °C with 11.8 μmol H_2 consumption, associated with the reduction of Pd species. The reduction temperature is much higher than that of Pd/Al_2O_3, indicating a strong interaction between Pd and Y-modified support. The findings suggest that there is a better Pd dispersion and smaller Pd size for $Pd5Y/Al_2O_3$ than Pd/Al_2O_3, in line with their XRD and CO-chemisorption results. In addition to the reduction peak, a small and wide peak between ~261 and 467 °C is also observed. The observation could be attributed to the H_2 reduction of partial Y_2O_3 promoted via a hydrogen spillover mechanism

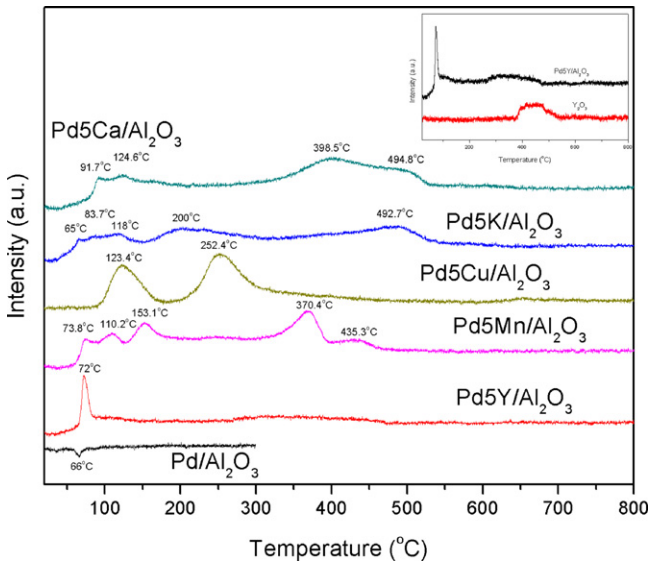

Fig. 2. H_2-TPR profiles of various catalysts (test conditions: 5% H_2/N_2 flow rate = 25 ml/min; heating rate = 10 °C/min).

from metal Pd to support, since pure Y_2O_3 can be partially reduced in a range of elevated temperatures, i.e. between 378 and 536 °C (see the insert of Fig. 2). According to some previous reports [30,31], which pointed out the partial reduction and surface oxygen mobility of Y_2O_3 as well as noble metal promotion effect, the present result implies that the surface oxygen vacancy and oxygen mobility in the lattice of the introduced Y_2O_3 is greatly improved by metal Pd as compared to that of pure Y_2O_3.

For $Pd5Cu/Al_2O_3$, the low and high temperature peaks at 123.4 and 252.4 °C consume 29.2 and 52.6 μmol H_2, respectively, and the first peak can be ascribed to the reduction of Pd–Cu alloy precursor and the second one to CuO. The reduction products are also confirmed by the present XRD results (Fig. 1). The literature reported similar results [29].

In agreement with previous studies [23,32], the three well-defined low temperature peaks at 73.8, 110.2 and 153.1 °C in the $Pd5Mn/Al_2O_3$ profile could be associated with the reduction of Pd oxides, whereas the high temperature ones at 370.4 and 435.3 °C could be assigned to the reductions of Mn oxides, which is confirmed to be MnO_2 and Mn_2O_3 by the XRD results of freshly calcined sample (not shown here), to Mn_3O_4 via Mn_2O_3 and Mn_3O_4 to MnO, respectively. The final reduction species, MnO, from Mn precursor is also evidenced by the XRD result (Fig. 1). The reductions of the Pd and Mn oxides consume 12.7 and 26.6 μmol H_2, respectively. For $Pd5Ca/Al_2O_3$, the high temperature peaks at 398.5 and 494.8 °C with a total of 35.7 μmol H_2 consumption could be assigned to the reduction of undecomposed Ca nitrate, as it is more difficult to reduce than Pd oxides [33]. Therefore, the low temperature peaks at 91.7 and 124.6 °C, which correspond to 9.1 μmol H_2 consumption, could be associated with the reduction of Pd oxides. Similarly, the high temperature peak at 492.7 °C in the $Pd5K/Al_2O_3$ profile could be assigned to H_2 consumption for the reduction of undecomposed KNO_3 to metal oxide, and the three low temperature peaks at 65.0, 83.7 and 118.0 °C, respectively, for the reduction of Pd oxides. Following the Pd reduction, subsequent H_2 consumption appears in the range of 150–325 °C. It was reported that the reduction temperature of KNO_3 on SiO_2 can shift to 190–430 °C from 450 to 730 °C when noble metal Ru was added to KNO_3/SiO_2 [28]. Accordingly, it is reasonable to assign the peak to the hydrogen reduction of KNO_3 species existing in the vicinity of Pd species. The reductions of the Pd oxides and KNO_3 consume 9.5 and 32.9 μmol H_2, respectively.

In addition, the broad and well-defined multi-peaks of Pd reduction over Ca, K, Cu and Mn-modified catalysts further suggests non-uniform Pd particle distribution, alloy formation and/or the occurrence of apparent decoration effect on catalysts. The decoration effect is caused by the close contact between the additive and Pd species. The close contact improves the reduction of additive species assisted by a spillover mechanism, in which hydrogen is transferred from metal Pd to additive.

3.2. Initial activity of catalysts

The control tests with the CO_2 reforming of CH_4 over Al_2O_3 and additive-modified Al_2O_3 confirm no observable conversions of CH_4 and CO_2, indicating that the reaction only takes place over the reduced Pd species. The initial activities of all Pd catalysts are investigated for the reaction in the range of 500–700 °C. Fig. 3 shows the conversion of CO_2 as a function of reaction temperature for all catalysts under reforming conditions. The initial activity strongly depends on the effect caused by the addition of different additives to Pd/Al_2O_3. Y and Ca show a positive effect whereas a negative effect is caused by Mn, K and Cu. The highest initial activity, expressed as CO_2 conversion ranging from 39.5% at 500 °C to 92.9% at 700 °C, is determined for $Pd5Y/Al_2O_3$, followed by $Pd5Ca/Al_2O_3$, Pd/Al_2O_3, $Pd5Mn/Al_2O_3$, $Pd5K/Al_2O_3$ and $Pd5Cu/Al_2O_3$. $Pd5Cu/Al_2O_3$ shows the largest activity decrease in

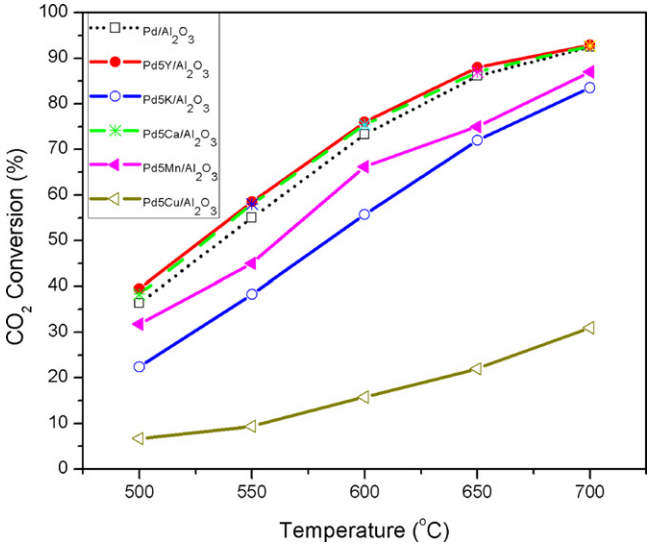

Fig. 3. The effect of reaction temperature on the initial CO_2 conversion of catalysts in dry reforming of CH_4 (reaction conditions: GHSV = 24,000 h^{-1}, $CH_4/CO_2/He$ = 1:1:2, P = 1 atm).

the whole temperature range, with its initial CO_2 conversions at 500, 600 and 700 °C, respectively, decrease by 30%, 57.5% and 61.5%, as compared to that of Pd/Al_2O_3. A similar trend for all catalysts can also be observed for initial CH_4 conversion (Fig. 4). When the reaction temperature reaches 700 °C, the initial activities for $Pd5Y/Al_2O_3$, $Pd5Ca/Al_2O_3$ and Pd/Al_2O_3 catalysts do not show noticeable difference among them, suggesting that the initial activity at elevated temperature for these catalysts display a more significant dependence on reaction temperature than the catalyst composition. This can be understood considering the strong endothermic nature of the reaction. These three catalysts seem to show larger abilities to convert both CH_4 and CO_2 than the recently reported 7.5 wt.% PdNi (80:20) ZrO_2-La_2O_3 catalyst in the reaction temperature range of 500–700 °C [18]. Moreover, the initial conversions of both CH_4 and CO_2 for these three catalysts are slightly higher than the thermodynamic equilibrium values in the whole temperature range. This could be due to the simultaneous

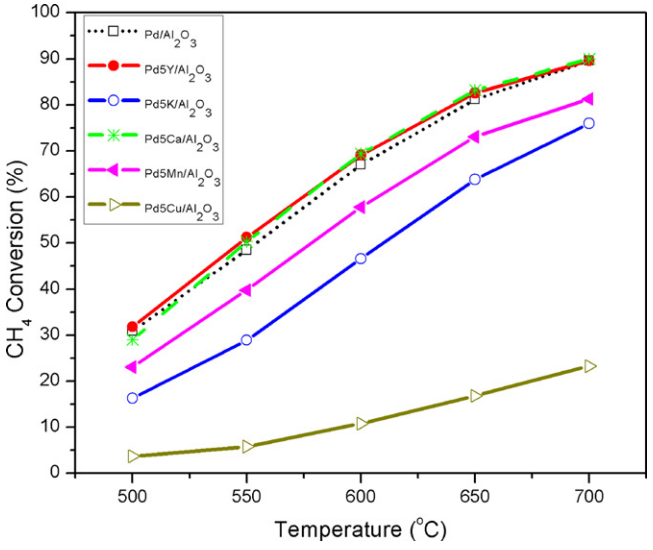

Fig. 4. The effect of reaction temperature on the initial CH_4 conversion of catalysts in dry reforming of CH_4 (reaction conditions: GHSV = 24,000 h^{-1}, $CH_4/CO_2/He$ = 1:1:2, P = 1 atm).

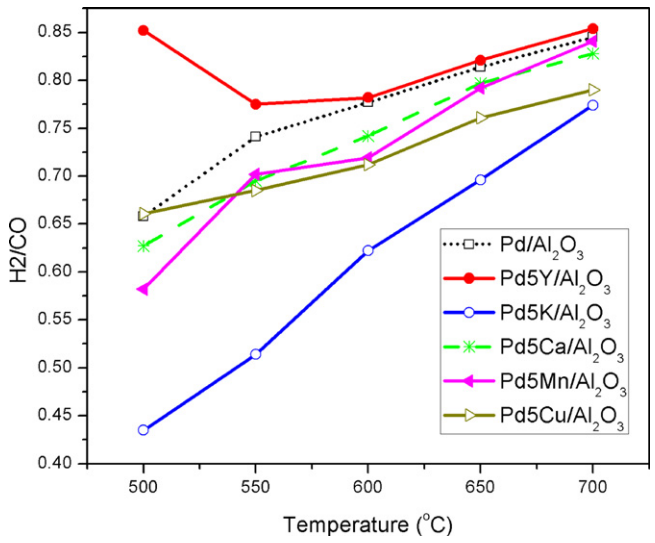

Fig. 5. The H_2/CO ratio as a function of reaction temeperature over Pd catalysts.

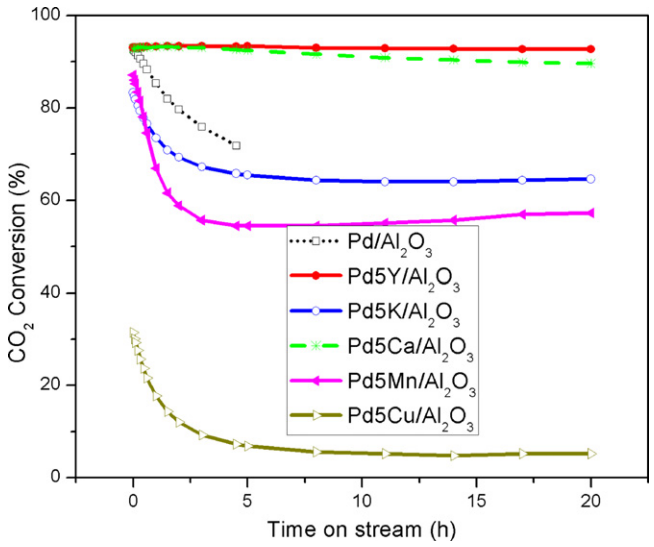

Fig. 6. The effect of reaction time on the CO_2 conversion of catalysts in dry reforming of CH_4 (reaction conditions: GHSV = 24,000 h^{-1}, $CH_4/CO_2/He$ = 1:1:2, P = 1 atm, T = 700 °C).

occurrence of some possible side reactions such as reverse water–gas shift reaction (RWGS, $CO_2 + H_2 \rightarrow H_2O + CO$), Boudouard reaction ($CO_2 + C \rightarrow 2CO$) and methane cracking ($CH_4 \rightarrow C + 2H_2$) [9,34]. Bouarab et al. [35] has reported a similar finding for Mg-modified Co/SiO_2 catalyst. On the other hand, for all catalysts the CO_2 conversion is always higher than the CH_4 conversion, even though CO_2 and CH_4 remain a stoichiometric ratio (1:1) in the feed gas. This further indicates that the RWGS occurs along with the reforming process. The RWGS is also responsible for the observation that the H/CO ratio, expressed as the ratio of H_2 and CO selectivities, is always less than 1 as shown in Fig. 5. The highest H_2/CO ratio is found over $Pd5Y/Al_2O_3$ as compared to others, suggesting a high H_2 selectivity and formation rate over this catalyst. The H_2/CO ratio increases as the increase of the reaction temperature regardless of the type of catalysts. This could be ascribed to the thermodynamic effect of RWGS reaction, which gradually becomes limited as the reaction temperature increases [1]. It was reported that the RWGS reaction is thermodynamically favorable and rapid to reach equilibrium under the reaction temperature between 500 and 700 °C [36,37]. Based on the thermodynamic equilibrium calculation, the conversions of CO_2 and CH_4 in the reforming process increase with increasing reaction temperature, and therefore there exists a high unconverted CO_2 concentration at a relatively low reaction temperature (<650 °C) and a low unconverted CO_2 concentration at high temperature (700 °C). Apparently, at low reaction temperature the high unconverted CO_2 concentration favors the RWGS forward reaction, leading to a low H_2/CO ratio as well as higher CO_2 conversion than CH_4 conversion. At high temperature the RWGS reaction becomes insignificant due to low unconverted CO_2 concentration, leading to close conversions of CO_2 and CH_4 and the H_2/CO ratio approaching one. Accordingly, both higher CO_2 conversion than CH_4 conversion and lower H_2/CO ratio are more obvious at low temperature than at high temperature.

3.3. Reaction stability of catalysts

Fig. 6 shows the conversion of CO_2 as a function of reaction time on stream at 700 °C. Pd/Al_2O_3 suffers from continuous and fast deactivation, and its CO_2 conversion level decreases from 92% to 71.9% within 4.5 h of time on stream, and thereafter the reaction drastically stops due to a large amount of accumulated carbon species blocking catalyst active bed. $Pd5K/Al_2O_3$ and $Pd5Mn/Al_2O_3$ catalysts display a similar deactivation pattern.

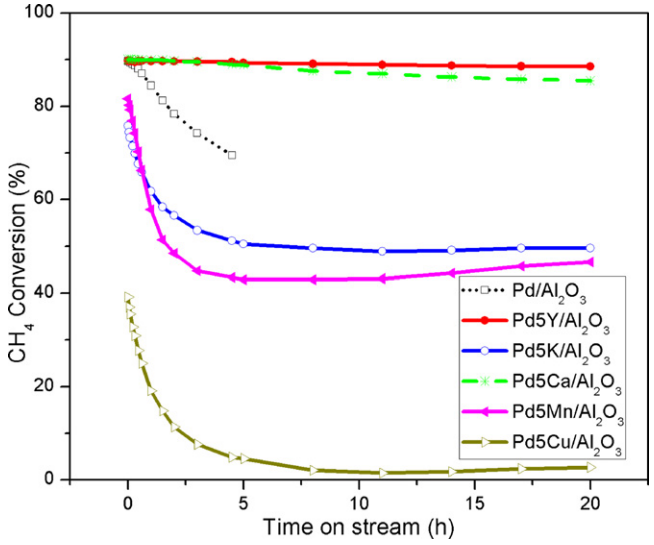

Fig. 7. The effect of reaction time on the CH_4 conversion of catalysts in dry reforming of CH_4 (Reaction conditions: GHSV = 24,000 h^{-1}, $CH_4/CO_2/He$ = 1:1:2, P = 1 atm, T = 700 °C).

Their CO_2 conversions decline quickly in the first 3 h and then remain constant at 64% and 58% until the end of test, respectively. The activity over $Pd5Ca/Al_2O_3$ maintains a decent stability. The CO_2 conversion only decreases by ~5% in the whole testing period. The best activity stability is found for $Pd5Y/Al_2O_3$, whose almost constant CO_2 conversion (93.5%) is the highest while on stream of 20 h. This observation is quite different from a recent study for nanostructured 1 wt.% Pt/Al_2O_3 catalyst with similar reforming conditions [21]. In the case of $Pd5Cu/Al_2O_3$, the CO_2 conversion decreases from 31% to 5% within ~5 h and then remains constant. The catalyst almost loses its activity completely after 5 h of reaction time, probably due to Pd–Cu alloy formation resulting in much less accessible Pd active sites. Based on these observations, the order of activity stability in terms of CO_2 conversion is $Pd/Al_2O_3 \sim Pd5Cu/Al_2O_3 < Pd5Mn/Al_2O_3 < Pd5K/Al_2O_3 < Pd5Ca/Al_2O_3 < Pd5Y/Al_2O_3$. The CH_4 conversion follows a similar pattern for all catalysts in the long-term stability test (Fig. 7). For every catalyst a higher CO_2 conversion is observed, compared to the

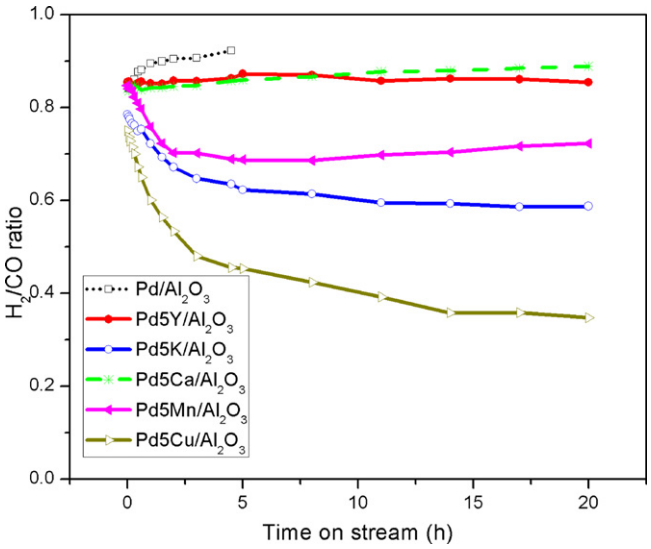

Fig. 8. The H_2/CO ratio as a function of reaction time over Pd catalysts.

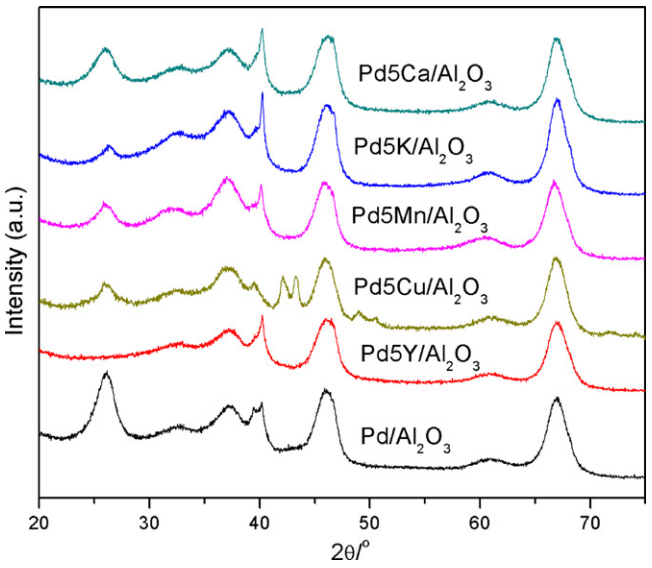

Fig. 9. The XRD patterns of spent catalysts after stability test of CH_4 reforming with CO_2.

CH_4 conversion, with the difference being 2% to 15% depending on the samples. As stated above, the observation can be associated with the simultaneous occurrence of RWGS reaction. The side reaction also accounts for the findings that the average H_2/CO ratio for all catalysts is less than 1, deviating from the stoichiometric value of unity, as shown in Fig. 8. A relatively constant H_2/CO ratio can be seen for $Pd5Y/Al_2O_3$ and $Pd5Ca/Al_2O_3$ catalysts throughout the testing period. The finding is in line with their high activity stabilities in terms of CH_4 and CO_2 conversions. However, for other catalysts the H_2/CO ratio shows either slight increase (Pd/Al_2O_3) or decrease ($Pd5Mn/Al_2O_3$, $Pd5K/Al_2O_3$ and $Pd5Cu/Al_2O_3$) as the reaction time increases, which could be due to their different activity decays resulting in different H_2 and CO selectivity.

3.4. Characterization of catalysts after long-term stability test

The textural properties of the catalysts after reaction are listed in Table 1. The surface area, pore volume and pore size of spent catalysts generally show lower values after the reaction. The decrease could be attributed to thermal sintering effect and/or carbon deposition effect. However, $Pd5Y/Al_2O_3$ displays the best stability toward thermal sintering.

Fig. 9 depicts the XRD patterns of the spent catalysts. Compared with fresh catalysts, the spent ones show stronger X-ray diffraction peaks related to Pd-containing species at $2\theta = 40.1^\circ$, suggesting the occurrence of Pd-containing crystallite sintering during the reforming reaction. The average Pd crystallite sizes of the spent catalysts, as calculated by Scherrer equation using the diffraction peaks of (1 1 1) plane of metal Pd at $2\theta = 40.1^\circ$, are 28.6, 10.6, 26.4, 16.7 and 20.7 nm for Pd/Al_2O_3, $Pd5Y/Al_2O_3$, $Pd5K/Al_2O_3$, $Pd5Ca/Al_2O_3$ and $Pd5Mn/Al_2O$, respectively (Table 2). For $Pd5Cu/Al_2O_3$, the average particle size of Pd–Cu alloy ($2\theta = 42.1^\circ$) is around 18.6 nm. Meanwhile, much weaker peak at $2\theta = 43.3^\circ$, a major indicator for metal Cu, is more pronounced in spent $Pd5Cu/Al_2O_3$ than the fresh one, which may be related to the size effect of Cu crystallites or surface carbon deposition on catalyst after reaction. For a similar reason, it is observed that the XRD signals of MnO for $Pd5Mn/Al_2O$ disappear. On the other hand, except $Pd5Y/Al_2O_3$, all spent catalysts show an apparent characteristic peak at $2\theta = 26.1^\circ$, designated to crystalline graphitic carbon (JCPDS 89-8491). The extremely strong and wide carbon signal over Pd/Al_2O_3 suggests a large amount of crystalline carbon species accumulated on the catalyst after the stability test.

Temperature-programmed oxidation test under oxidative atmosphere is a useful technique to investigate the carbon deposition over spent catalysts, since it can offer some important information about the accumulated carbon species in the CH_4 reforming process, such as carbon structure, amount and composition etc. It is widely accepted that amorphous carbon species can be combusted at lower temperature than crystalline ones, and the oxidation temperature increases with the increasing degree of crystallinity [38,39]. Generally, amorphous carbon species could be combusted below 500 °C, whereas crystalline ones at temperature above 520 °C [38,39]. Fig. 10 displays the signal of generated CO_2 as a function of rising catalyst bed temperature. The TPO profile of Pd/Al_2O_3 shows the widest and strongest CO_2 release peak in the temperature range of 400–840 °C as compared to that of other catalysts. The wide peak is mainly associated with the combustion of carbon species of different crystalline forms, e.g. carbon nanofibers (CNFs) and carbon nanotubes (CNTs), etc.

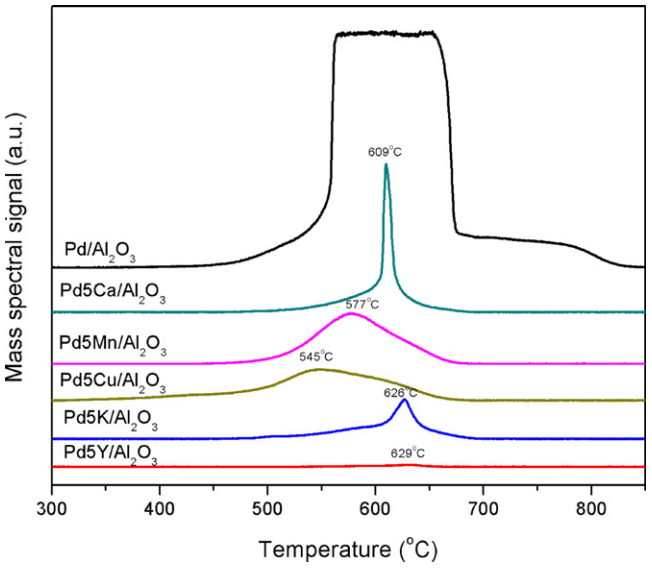

Fig. 10. The TPO profiles of spent catalysts after stability test of CH_4 reforming with CO_2.

Table 3
Amount, formation rate and Raman property of carbon deposition on spent catalysts.

Catalyst	Amount of carbon deposition (g_c/g_{cat})	Average carbon formation rate ($g_c/(g_{cat}$-h))	Relative intensity ratio of D and G bands on Raman spectra (I_D/I_G)
Pd/Al_2O_3	0.533	0.118	1.84
$Pd5Y/Al_2O_3$	Trace	–	0.88
$Pd5K/Al_2O_3$	0.028	0.0014	1.26
$Pd5Ca/Al_2O_3$	0.080	0.004	1.37
$Pd5Mn/Al_2O_3$	0.100	0.005	1.62
$Pd5Cu/Al_2O_3$	0.100	0.005	2.44

Carbon deposition in CO_2 reforming of CH_4 develops on the surface of metal particles through two routes: (i) methane decomposition to carbon and hydrogen ($CH_4 \rightarrow C + 2H_2$), and (ii) disproportionation of carbon monoxide to carbon and carbon dioxide ($2CO \rightarrow C + CO_2$) [40,41]. The small amount of CO_2 release below 500 °C arises from oxidation of carbon, which is formed mainly via CH_4 decomposition, while the large amount of CO_2 release above 500 °C comes from oxidation of coke, which is deposited through CO disproportionation [42,43]. All additive-added catalysts present much less CO_2 release signals on their TPO profiles than Pd/Al_2O_3, indicating the strong effect of additives in reducing carbon deposition on the catalyst. The maximum temperature values of CO_2 release peak are shifted to 545, 577, 609, 626 and 629 °C for $Pd5Cu/Al_2O_3$, $Pd5Mn/Al_2O_3$, $Pd5Ca/Al_2O_3$, $Pd5K/Al_2O_3$ and $Pd5Y/Al_2O_3$, respectively. The temperature increase order corresponds to increasing degree of crystallinity of carbon species on these spent catalysts. The total amount of carbon deposition as well as corresponding carbon formation rate for spent catalyst is estimated from the amount of the released CO_2 from the TPO test as listed in Table 3. It can be seen that both the carbon deposition amount and coke formation rate follow the order: $Pd/Al_2O_3 > Pd5Cu/Al_2O_3 \sim Pd5Mn/Al_2O_3 \sim Pd5Ca/Al_2O_3 > Pd5K/Al_2O_3 > Pd5Y/Al_2O_3$. Pd/Al_2O_3 shows the largest carbon amount and the highest carbon formation rate being 0.533 g_c/g_{cat} and 0.118 g_c/g_{cat}-h, respectively, whereas only trace carbon is formed on $Pd5Y/Al_2O_3$ during 20 h of reaction. On the other hand, we note that no measurable amount of water was detected for all performed TPO tests. It can therefore be inferred that the deposited carbon species during stability test of the reforming of CH_4 do not contain hydrocarbons.

The structure and composition of crystalline carbon species deposited on spent catalysts are further characterized by Raman spectroscopy, and the results are shown in Fig. 11. All Raman spectra of spent catalysts show two well-defined bands at around 1332 and 1592 cm^{-1}, respectively. The former is the so-called D band, associated with the disordered structural mode of crystalline carbon species, whereas the latter is known as G band, which is related to graphitic carbon with high degree of symmetry and order [21,43,44]. It has been known that the relative intensity (I_D/I_G) of D and G bands is an indicator of the degree of order for crystalline carbon species. Smaller I_D/I_G value means higher crystallinity of graphite [45,46]. The I_D/I_G values of catalysts are calculated and listed in Table 3. The Y and Cu-added catalysts show the smallest and largest I_D/I_G values being 0.88 and 2.44, respectively, and all I_D/I_G values decrease in the order: $Pd5Cu/Al_2O_3 > Pd/Al_2O_3 > Pd5Mn/Al_2O_3 > Pd5Ca/Al_2O_3 > Pd5K/Al_2O_3 > Pd5Y/Al_2O_3$. This suggests that the increase of graphitization degree on spent catalysts follows the same trend. The result coincides with the increasing oxidation temperatures of carbon deposition on the spent catalysts in the TPO tests. In addition, the I_D/I_G value of $Pd5Y/Al_2O_3$ is less than 1, suggesting that more well-ordered graphite carbon is present on the spent catalyst than disordered carbon species. On the contrary, other catalysts, of which I_D/I_G values are between 1.26 and 2.44, show much more disordered carbon species than well-ordered graphitic carbon.

Pd distribution and carbon deposition over the catalysts obtained after catalytic stability tests are observed by TEM technique. The representative results are shown in Fig. 12. The γ-Al_2O_3 support shows well-defined nanofiber structure. Pd particle size distribution over spent Pd/Al_2O_3 is found in a wide range from ~8 to 160 nm, with a considerable amount of particles with diameter >60 nm. This is due to a significant metal sintering occurs during the reaction. Pd particles over spent $Pd5Ca/Al_2O_3$ are found to be between ~5 and 25 nm, whereas spent $Pd5K/Al_2O_3$ displays Pd particle sizes of 10–40 nm. For Mn-modified catalyst, some Pd particles with 80–110 nm can be seen in addition to noticeable small ones of 12–20 nm. Most notably, metal particles presented on spent $Pd5Y/Al_2O_3$ distribute fairly uniformly, where Pd particle size mostly falls between 5 and 10 nm, with only a couple of particles of ~12 nm. These promoters can suppress Pd sintering to different degrees since they strengthen the interaction between Pd and the support. As for spent $Pd5Cu/Al_2O_3$, very large metal particles up to 300 nm are observed due to Pd–Cu alloy sintering under the reaction conditions.

On the other hand, carbon accumulation can be observed on all spent catalysts from Fig. 12. The carbon deposition, which accumulates on metal particles and indicates a tip-growth mode, is mainly in the form of filaments (CNTs, CNFs and/or graphite). The grown carbon filaments have the same diameters as the attached metal particles. This is in agreement with literatures showing a strong correlation between metal particle size and grown carbon filament [47,48]. Spent Pd/Al_2O_3 displays much heterogeneity of carbon filaments with a wide range of diameters depending on

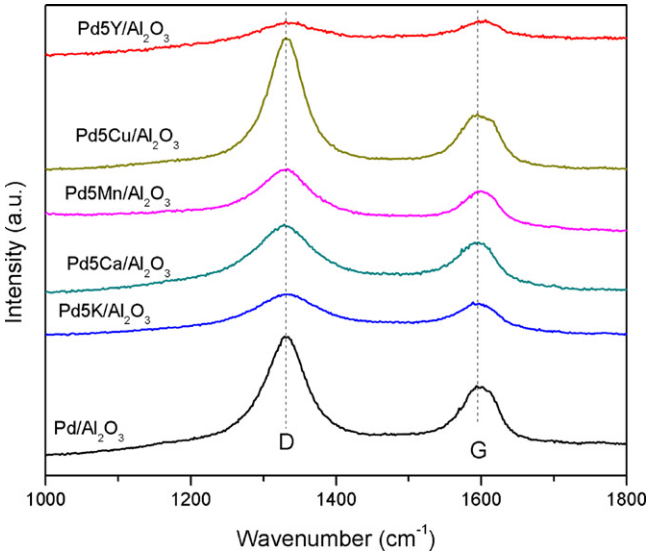

Fig. 11. Raman spectra of spent catalysts after stability test of CH_4 reforming with CO_2.

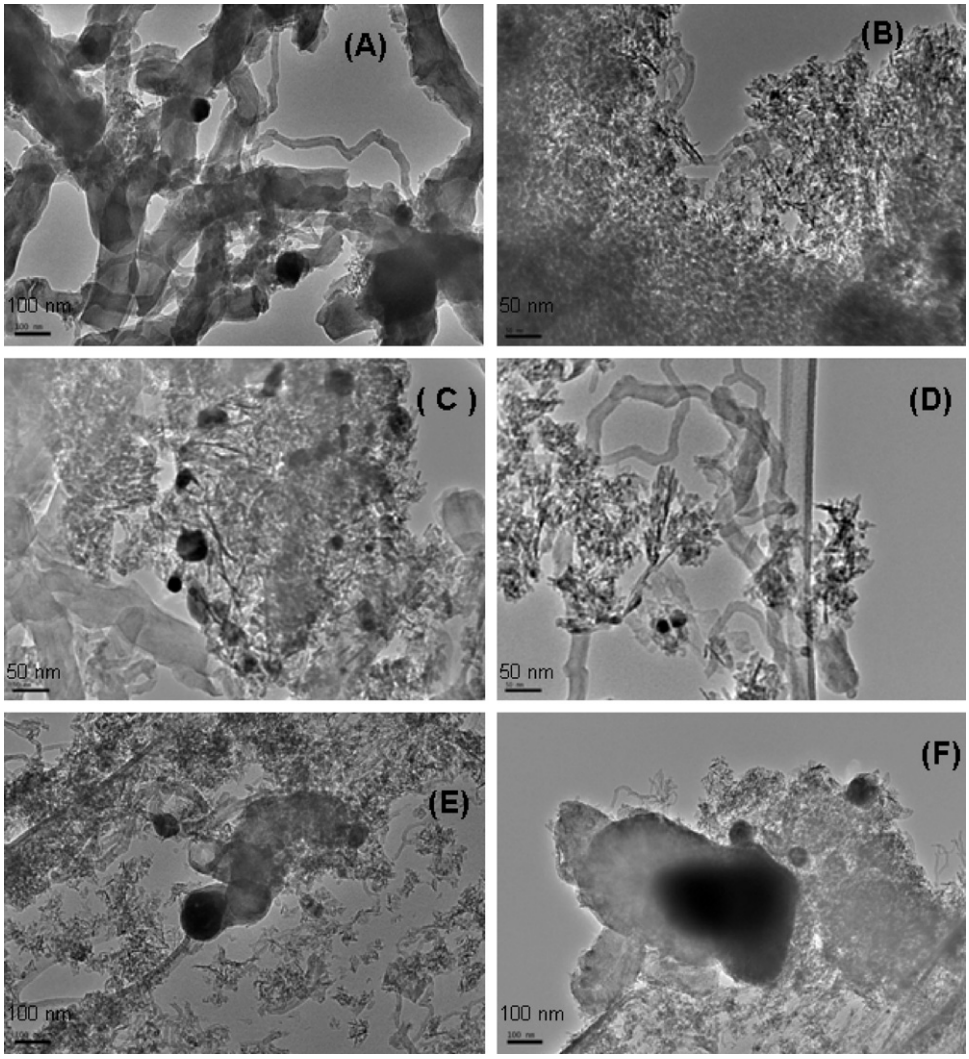

Fig. 12. TEM images of spent catalysts after stability test of CH_4 reforming with CO_2 (A) Pd/Al_2O_3; (B) $Pd5Y/Al_2O_3$; (C) $Pd5Ca/Al_2O_3$; (D) $Pd5K/Al_2O_3$; (E) $Pd5Mn/Al_2O_3$; (F) $Pd5Cu/Al_2O_3$.

Pd particle sizes. The carbon formation over spent $Pd5Y/Al_2O_3$, which only contains a few short and small CNTs with diameter of ~12 nm, is significantly suppressed due to highly dispersive Pd particles with sizes of <10 nm. Apparently, such small Pd particles do not favor carbon filament growth. Meanwhile, it is clear that the forms of carbon deposition are CNTs and CNFs for both spent $Pd5Ca/Al_2O_3$ and $Pd5K/Al_2O_3$, whereas mainly CNTs and graphite for both $Pd5Mn/Al_2O_3$ and $Pd5Cu/Al_2O_3$. The presence of graphite over the Mn or Cu-modified catalysts indicates relatively loosened carbon structure and high crystalline imperfections of deposited coke. This also indirectly supports the argument that carbon deposition on the two spent catalysts can be combusted under relatively low temperatures (Fig. 10) and their Raman spectra display relatively high I_D/I_G values (Fig. 11). In addition, we note that no carbon filament is formed on some metal particles with size >15 nm for spent catalysts with K, Ca, Mn or Cu additives. This observation could be attributed to either metal particle covered by added promoter component or formation of metal Cu particles, which is not active for the dry reforming of CH_4.

3.5. Origin of catalyst deactivation

Mechanistic studies suggest that CO_2 reforming of CH_4 start at the decomposition of methane over active metallic sites [1,2,4,16,37,49–51]. Accessible Pd particles act as the active sites. Therefore, sufficient accessible active Pd sites and strong metal sintering resistance are key factors in maintaining the high activity and stability of catalysts under harsh reforming conditions. The XRD and TEM observations of spent catalysts demonstrate that addition of Y, Ca, K and Mn to Pd/Al_2O_3 suppresses the generation of large Pd particle and improves the uniformity of metal distribution to different extent under long-term reforming conditions, while Cu additive leads to the marked decrease of Pd dispersion, which is ascribed to the formation of large Pd–Cu alloy particles. On the basis of the XRD and TEM results it can be concluded that the ability of sintering resistance follows the order: $Pd5Y/Al_2O_3 > Pd5Ca/Al_2O_3 > Pd5K/Al_2O_3 > Pd5Mn/Al_2O_3 > Pd/Al_2O_3 > Pd5Cu/Al_2O_3$. $Pd5Y/Al_2O_3$ and $Pd5Ca/Al_2O_3$ maintain high conversions of CH_4 and CO_2, which could be attributed to their high metal sintering resistance. Significant Pd sintering over Pd/Al_2O_3 contributes to the continuous decrease of catalyst activity in term of conversions in the 4.5 h period on stream. For $Pd5K/Al_2O_3$, $Pd5Mn/Al_2O_3$ and $Pd5Cu/Al_2O_3$, apparent metal or alloy sintering as well as decoration effect greatly decreases exposed Pd active sites and results in lower activity stabilities on stream.

Surface carbon deposition is another important factor related to catalyst deactivation during CO_2 reforming of CH_4. Many mechanistic studies have suggested that excessive carbon deposition occur

when the generation rate of carbon species on the catalyst surface is faster than its removal rate [4,37,49–51]. It is believed that carbon deposition deactivates catalysts by covering accessible metal active sites, which is responsible for the occurrence of the reaction. The deactivation is closely related to the amount, deposition rate and forms of coke accumulated on the catalysts. The largest carbon deposition and the fastest coking rate over Pd/Al_2O_3 result in its full deactivation in a short reforming time, whereas the best activity stability is found for $Pd5Y/Al_2O_3$, which only shows trace carbon deposition. However, when one correlates carbon deposition amount with catalytic stability, it can be found that large amount of carbon does not always lead to larger activity loss in terms of the CH_4 and CO_2 conversions. For example, $Pd5Cu/Al_2O_3$, $Pd5Mn/Al_2O_3$ and $Pd5Ca/Al_2O_3$ show similar amounts of carbon deposition but the CH_4 and CO_2 conversions follow the order: $Pd5Ca/Al_2O_3 > Pd5Mn/Al_2O_3 > Pd5Cu/Al_2O_3$. $Pd5K/Al_2O_3$ presents significantly less carbon deposition than $Pd5Mn/Al_2O_3$, but they have similar catalytic stability. These results suggest that accumulated carbon species is an important but not the only factor to cause the deterioration of catalytic stability.

For the present Pd catalyst system, TEM results show that carbon depositions grow on metal particles and exist in the form of filaments, i.e. CNTs, CNFs, and loosened graphite. The carbon filaments do not directly affect the activity and stability of active component on catalysts negatively. However, a large amount of the carbon species, especially loosened graphite, would cover large surface, block catalyst bed and eventually stop the reforming reaction due to the loss of accessible active metal sites on catalyst. This is why the dry reforming abruptly stops over Pd/Al_2O_3 after 4.5 h on stream while the conversions of CH_4 and CO_2, around 70% and 72% respectively, still remain at decent levels. Thus, the deactivation for Pd/Al_2O_3 catalysts with Ca, K, Mn and Cu modifications can be largely attributed to decreased active Pd sites due to either metal particle sintering or active sites partially covered by carbon formation. It is generally accepted that the carbon species chemically adsorbed on small metal particles is more difficult to diffuse and grow than those on large particles [52]. This means sintering accelerates the carbon deposition since large metal ensembles facilitate coke formation [7,53]. Therefore, the formation of carbon filaments strongly depends on metal particle size, in agreement with many reports in the literature [47,48]. Depending on the different kinds of catalysts, the biggest particle sizes, such as 11.5 nm for bimetallic PdNi/MCM-41 [54], 7 nm for monometallic La_2NiO_4 catalyst [55], and 7 nm for Ni–alumina aerogel [56], respectively, have been suggested to completely suppress carbon formation in dry reforming of methane. Present TEM results for both Pd/Al_2O_3 and $Pd5Y/Al_2O_3$, which show no decoration effect, confirm that there exists a similar threshold value for Pd particle size (~10 nm), below which carbon formation could be completely avoided during reaction. This threshold value of Pd particle size was not reported before.

Addition of Y_2O_3 to Pd/Al_2O_3 significantly suppresses both surface Pd sintering and coke deposition, resulting in superior activity stability and high conversions of CH_4 and CO_2. This is attributed to the promotion effect of Y_2O_3 on Pd/Al_2O_3. According to the results of XRD, H_2-TPR and CO-chemisorption, it can be concluded that there is no decoration effect between Pd and Y_2O_3. This means that the existence of small Pd particles over $Pd5Y/Al_2O_3$ is related to the "dilution" or "segregation" effect of Y_2O_3. The effect greatly increases exposed Pd–Y interfacial area where reforming of CH_4 occurs. Moreover, the results of XRD, H_2-TPR and TEM demonstrate that Y_2O_3 highly disperse over the catalyst. The supported small Y_2O_3 particles are apt to easily form surface oxygen vacancy and increase oxygen mobility through the lattice, as demonstrated by the H_2-TPR result that the supported Y_2O_3 is much easier to be partially reduced than the corresponding non-supported oxide. The characteristic of Y_2O_3 may play an important role in activating CO_2 and cleaning carbon deposition on the metal Pd. The adsorption and dissociation of CO_2 over the oxygen vacancy of Y_2O_3 lead to the formation of CO and active oxygen. The produced oxygen enters the lattice of Y_2O_3, then migrates to the Pd–Y interface via oxygen mobility and finally reacts with CH_x, a decomposition product of CH_4 on metal Pd, to effectively remove carbon deposition. Similar results have been observed over Y_2O_3-, CeO_2- and La-doped Ni or Pt/ZrO_2 catalysts for dry reforming of methane [8,11,57–59].

4. Conclusion

The selected additives, Y, Ca, K, Mn and Cu, have no remarkable effect on the texture properties of Pd/Al_2O_3, but significantly affect the surface Pd dispersion and metal sintering resistance, resulting in different extents of carbon deposition and catalytic performance during CO_2 reforming of CH_4. Pd/Al_2O_3 shows high initial activity but poor stability in terms of CH_4 and CO_2 conversions due to severe Pd sintering and a large amount of carbon deposition. $Pd5Y/Al_2O_3$ exhibits the highest initial activity in the reaction temperature range of 500–700 °C and the best stability with no activity loss during 20 h on stream. We attribute this to its best Pd dispersion and the strongest ability of metal sintering resistance and coke resistance. The deactivation with different extents for Ca, K, Mn and Cu-modified Pd catalysts during stability test is ascribed to the amount, coking rate and forms of carbon deposition, as well as the sintering of accessible active Pd sites. Moreover, 10 nm is suggested as a critical Pd particle size for present reforming conditions, below which carbon deposition can be totally suppressed.

Acknowledgments

Support from the US Department of Energy (DE-FC26-05NT42457) and the Natural Science Foundation (CHE-0632071) are gratefully acknowledged.

References

[1] M.C.J. Bradford, M.A. Vannice, Catal. Rev. Sci. Eng. 41 (1999) 1.
[2] Y.H. Hu, E. Ruckenstein, Adv. Catal. 48 (2004) 297.
[3] J.-S. Chang, S.-E. Park, J.W. Yoo, J.-N. Park, J. Catal. 195 (2000) 1.
[4] E. Ruckenstein, H.Y. Wang, J. Catal. 205 (2002) 289.
[5] X. Zhu, P. Huo, Y. Zhang, D. Cheng, C. Liu, Appl. Catal. B 81 (2008) 132.
[6] J.S. Chang, S.E. Park, H. Chon, Appl. Catal. A 145 (1996) 111.
[7] B.S. Liu, C.T. Au, Appl. Catal. A 244 (2003) 181.
[8] J.B. Wang, S.Z. Hsiao, T.J. Huang, Appl. Catal. A 246 (2003) 197.
[9] J. Zhang, H. Wang, A.K. Dalai, J. Catal. 249 (2007) 300.
[10] S.H. Seok, S.H. Choi, E.D. Park, S.H. Han, J.S. Lee, J. Catal. 209 (2002) 6.
[11] S.M. Stagg-Williams, F.B. Noronha, G. Fendley, D.E. Resasco, J. Catal. 194 (2000) 240.
[12] H.Y. Wang, E. Ruckenstein, Appl. Catal. A 204 (2000) 143.
[13] M. Masai, H. Kado, A. Miyake, S. Nishiyama, S. Tsuruya, Stud. Surf. Sci. Catal. 36 (1988) 67.
[14] F. Solymosi, A. Erdöhelyi, J. Cserényi, Catal. Lett. 16 (1992) 399.
[15] A. Erdöhelyi, J. Cserényi, E. Papp, F. Solymosi, Appl. Catal. 108 (1994) 205.
[16] A. Yamaguchi, E. Iglesia, J. Catal. 274 (2010) 52.
[17] P.G. Schulz, M.G. Gonzalez, C.E. Quincoces, C.E. Gigola, Ind. Eng. Chem. Res. 44 (2005) 9020.
[18] B. Steinhauer, M.R. Kasireddy, J. Radnik, A. Martin, Appl. Catal. A 366 (2009) 333.
[19] S. Damyanova, J.M.C. Bueno, Appl. Catal. A 253 (2003) 135.
[20] V.A. Tsipouriari, X.E. Verykios, Catal. Today 64 (2001) 83.
[21] M. García-Diéguez, I.S. Pieta, M.C. Herrera, M.A. Larrubia, L.J. Alemany, J. Catal. 270 (2010) 136.
[22] J. Batista, A. Pintar, J.P. Gomilek, A. Kodre, F. Bornette, Appl. Catal. A 217 (2001) 55.
[23] M.C. Álvarez-Galván, B. Pawelec, V.A. de la Peña O'Shea, J.L.G. Fierro, P.L. Arias, Appl. Catal. B 51 (2004) 83.
[24] H. Lieske, J. Voelter, J. Phys. Chem. 89 (1985) 1841.
[25] C. Shi, B. Jang, Ind. Eng. Chem. Res. 45 (2006) 5879.
[26] R. Pellegrini, G. Leofanti, G. Agostini, L. Bertinetti, S. Bertarione, E. Groppo, A. Zecchina, C. Lamberti, J. Catal. 267 (2009) 40.
[27] A.F. Gusovius, T.C. Watling, R. Prins, Appl. Catal. A 188 (1999) 187.
[28] M.G. Musolino, C.V. Caia, C. Busacca, F. Mauriello, R. Pietropaolo, Appl. Catal. A 357 (2009) 106.

[29] J. Batista, A. Pintar, D. Mandrino, M. Jenko, V. Martin, Appl. Catal. A 206 (2001) 113.
[30] G.B. Sun, K. Hidajat, X.S. Wu, S. Kawi, Appl. Catal. B 81 (2008) 303.
[31] F.B. Passos, E.R. Oliveira, L.V. Mattos, F.B. Noronhe, Catal. Lett. 110 (2006) 261.
[32] F. Kapteijn, A.D. Vanlangeveld, J.A. Moulijn, A. Andreini, M.A. Vuurman, A.M. Turek, J.M. Jehng, I.E. Wachs, J. Catal. 150 (1994) 95.
[33] Y. Shanmugam, F.Y. Lin, T.H. Chang, C.-T. Yeh, J. Phys. Chem. B 107 (2003) 1044.
[34] J.H. Edwards, A.M. Maitra, Fuel Process. Technol. 42 (1995) 269.
[35] R. Bouarab, O. Akdim, A. Auroux, O. Cherifi, C. Mirodatos, Appl. Catal. A 264 (2004) 161.
[36] M.M.V.M. Souza, D.A.G. Aranda, M. Schmal, J. Catal. 204 (2001) 498.
[37] J.R. Rostrup-Nielsen, J.H. Bak Hansen, J. Catal. 144 (1993) 38.
[38] Z. Yu, D. Chen, M. Rønning, B. Tøtdal, T. Vralstad, E. Ochoa-Fernandez, A. Holmen, Appl. Catal. A 338 (2008) 147.
[39] J.W. Long, M. Laskoski, T.M. Keller, K.A. Pettigrew, T.N. Zimmerman, S.B. Qadri, G.W. Peterson, Carbon 48 (2010) 501.
[40] M.C.J. Bradford, M. Albert Vannice, Appl. Catal. A 142 (1996) 73.
[41] H.M. Swaan, V.C.H. Kroll, G.A. Martin, C. Mirodatos, Catal. Today 21 (1994) 571.
[42] V.C.H. Kroll, H.M. Swaan, S. Lacombe, C. Mirodatos, J. Catal. 164 (1997) 387.
[43] D. Liu, X.Y. Quek, W.N.E. Cheo, R. Lau, A. Borgna, Y. Yang, J. Catal. 266 (2009) 380.
[44] H.B. Zhang, G.D. Lin, Z.H. Zhou, X. Dong, T. Chen, Carbon 40 (2002) 2429.
[45] Y. Liu, C. Pan, J. Wang, J. Mater. Sci. 39 (2004) 1091.
[46] C. Pan, Q. Bao, J. Mater. Sci. Lett. 21 (2002) 1927.
[47] T.V. Choudhary, E. Aksoylu, D.W. Goodman, Catal. Rev. Sci. Eng. 45 (2003) 151.
[48] D. Chen, K.O. Christensen, E. Ochoa-Fernández, Z. Yu, B. Tøtdal, N. Latorre, A. Monzón, A. Holmen, J. Catal. 229 (2005) 82.
[49] D. Qin, J. Lapszewicz, X. Jiang, J. Catal. 159 (1996) 140.
[50] J.H. Bitter, K. Seshan, J.A. Lercher, J. Catal. 176 (1998) 93.
[51] H.Y. Wang, C.T. Au, Appl. Catal. A 155 (1997) 239.
[52] J.R. Rostrup-Nielsen, Stud. Surf. Sci. Catal. 68 (1991) 85.
[53] X.E. Verykios, Int. J. Hydrogen Energy 28 (2003) 1045.
[54] S. Damyanova, B. Pawelec, K. Arishtirova, J.L.G. Fierro, C. Sener, T. Dogu, Appl. Catal. B 92 (2009) 250.
[55] G.S. Gallego, F. Mondragón, J. Barrault, J.M. Tatibouët, C. Batiot-Dupeyrat, Appl. Catal. A 311 (2006) 164.
[56] J.H. Kim, D.J. Suh, T.J. Park, K.L. Kim, Appl. Catal. A 197 (2000) 191.
[57] L. Pino, A. Vita, F. Cipitì, M. Laganà, V. Recupero, Appl. Catal. B 104 (2011) 64.
[58] H.S. Roh, H.S. Potdar, K.W. Jun, J.W. Kim, Y.S. Oh, Appl. Catal. A 276 (2004) 231.
[59] N. Laosiripojana, S. Assabumrungrat, Appl. Catal. B 60 (2005) 107.